Convection and thermodiffusion of colloidal gold tracers by laser light scattering

Wolfgang Schaertl* and Christopher Roos
Institut für Physikalische Chemie, Universität Mainz, Welderweg 11, 55099 Mainz, Germany
(Received 2 March 1999)

In a dynamic light scattering experiment, we have investigated the time intensity correlation function and the profile of the transmitted laser beam for organic dispersions of light absorbing colloidal particles containing tiny gold clusters. The correlation functions have been found to show a superposition of an exponential decay, corresponding to Brownian motion of the tracers, and well-defined oscillations. These oscillations are caused by convection due to local heating of the sample by the incident laser beam, which has been confirmed independently via measurements of the local temperature within the sample. It will be shown how the particle convection velocity, which is the order of 1 mm/s, can be obtained quantitatively from the oscillating correlation functions. The profile of the transmitted beam allowed us to determine the Soret coefficient, which is a measure for the thermal diffusion of the particles. This article shows how tracer diffusion, convection, and thermal diffusion can be determined simultaneously by one single experiment, laser light scattering of light absorbing colloidal particles in dispersion. [S1063-651X(99)09708-1]

PACS number(s): 47.27.Te, 42.25.Fx, 66.10.Cb, 71.24.+q

I. INTRODUCTION

Laser light scattering [1,2] nowadays is a very common tool to determine particle size and structure or to study particle mobility in soft condensed matter, as concentrated colloidal dispersions [3]. For the latter purpose, often special tracer methods have to be used, where the scattering efficiency of the tracer particles has to be much larger than that of the surrounding matrix. Therefore, the signal obtained in a light scattering experiment only reflects the dynamical (and static) properties of the tracers, which of course are influenced by the surrounding matrix. A suitable class of such tracers are light absorbing colloidal particles. As a consequence of their light absorption, those particles show a strong increase in scattering power, a phenomenon which is known as enhanced Rayleigh scattering [4]. However, the light absorption may cause unwanted side effects as local heating, convection and thermal diffusion. A detailed experimental and theoretical investigation of these side effects is the subject of the present paper.

Whereas light absorbing colloidal spheres labeled with organic dyes [5] are not appropriate tracers for standard laser light scattering due to irreversible destruction (bleaching) of the label upon irradiation, particles containing tiny gold clusters are very well suited: these tracers show light absorption as a quantum optical effect, and no bleaching of the gold clusters may occur. Liz-Marzan *et al.* [6] have tried to use gold clusters coated by a silica shell as tracers in dynamic light scattering experiments. They reported unusual deviations of the time intensity correlation functions in respect to the expected strictly exponential decay. More recently, we have reported on dynamic light scattering of polyorganosiloxane-μ gels [7–9], a new class of colloidal nanospheres soluble in nonpolar organic solvents up to very high concentrations, filled with tiny gold clusters [10]. We have found unusual oscillations in the correlation functions not reported before, which, at that time, had been attributed qualitatively to convection caused by local heating of the sample.

In this article, we provide a detailed analysis of the unusual light scattering effects found for colloidal dispersions of light absorbing polyorganosiloxane-μ gels. In the new experiments, we have used another class of gold-filled colloidal tracers each containing just one slightly larger gold cluster, leading to a strong enhancement of light absorption compared to the previous system.

The oscillations found in the correlation functions will be investigated in detail, showing that they provide a quantitative measure of the flux velocity. Especially, an analysis of the dependence of the oscillations on the scattering angle allows to localize the direction of the convection. Also, the local temperature within the sample has been measured, supporting the assumption of a finite roll pattern of the thermal convection. Such kind of convection pattern usually is found if a fluid system is heated from below [11–13].

Finally, it will be shown how the thermal diffusion and the Soret coefficient [14–16] can be determined from the profile of the transmitted beam, as described in a recent theoretical article [17]. In contrast to the theoretical model, the self-phase modulation has been found to be asymmetric in our case. This is caused by the effect of gravity, which has not been considered in [17], but plays an important role in experiments.

II. EXPERIMENT

A. Samples

Previously, polyorganosiloxane-μ gels of average diameter 50 nm, filled with several tiny gold clusters (sample *A*), have been investigated [10]. Here, we employed new tracer particles of average diameter (inverse *z*-average as determined by dynamic light scattering) 75 nm, containing one single larger gold cluster (sample *B*). As will be shown later, these new tracers have a strongly increased absorption com-

*Electronic address: wolfgang@hal2000.chemie.uni-mainz.de

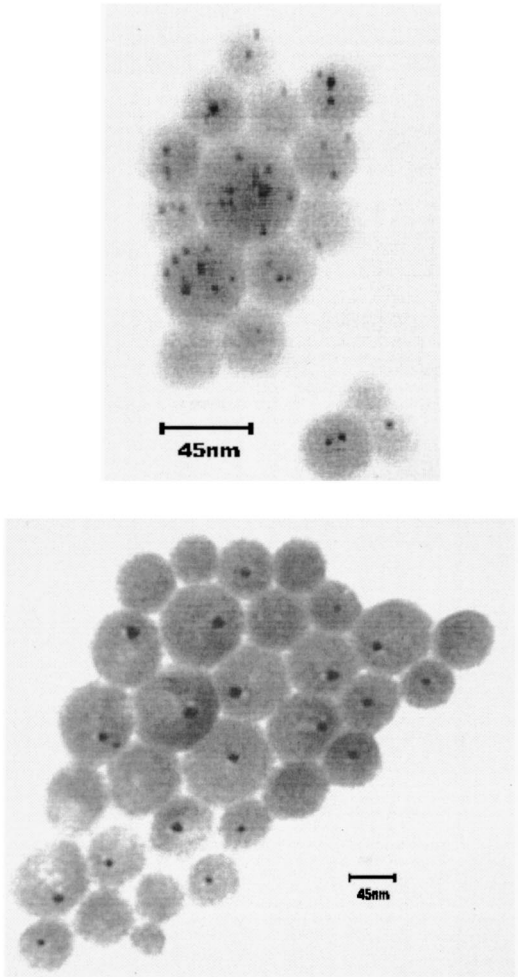

FIG. 1. Transmission electron micrographs of tracer systems *A* (top) and *B* (bottom). Black bars indicate a size scale of 45 nm.

pared to the former sample *A*, leading to a strong enhancement of convection and thermodiffusion studied in this article. Synthesis and detailed characterization of these particles are described elsewhere. Transmission electron micrographs of both tracer species are shown in Fig. 1.

The small gold clusters cause light absorption of these tracer particles in the regime $450<\lambda_{max}<550$ nm, depending on the actual size of the gold clusters. This leads to an enhancement of scattering power, if laser light close to the absorption band is used (enhanced Rayleigh scattering [4]). The uv-visible-absorption spectra of the tracers are shown in Fig. 2.

For the larger gold clusters (sample *B*), the absorption maximum is slightly shifted towards longer wavelength, as expected for optical quantum size effects. At the given wavelength of our Ar^+ laser indicated by the bar in Fig. 2 (514 nm, see below), the specific absorption of sample *A* is about 0.23 $g^{-1}\,l\,cm^{-1}$, whereas that of sample *B* is more than twice as large (0.55 $g^{-1}\,l\,cm^{-1}$). In the light scattering experiments, colloidal dispersions containing 0.2 wt. % tracer particles in the organic solvent cyclohexane have been studied. The particle concentration of 0.2 wt. % corresponds to an optical absorption $\sigma=0.46\ cm^{-1}$ for the former sample *A* and $\sigma=1.10\ cm^{-1}$ for the new sample *B*.

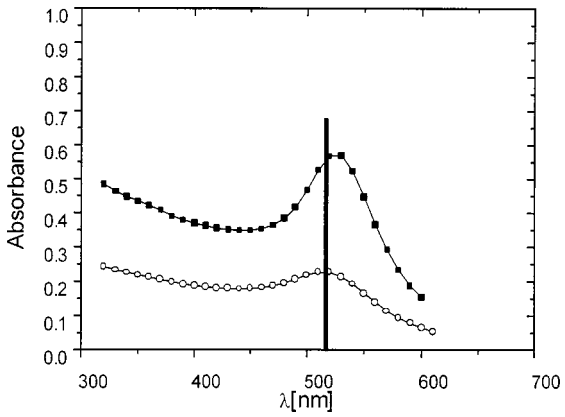

FIG. 2. uv-visible absorption spectra of tracer systems *A* (open symbols) and *B* (filled symbols) at tracer concentration 0.1 wt. %. The black bar indicates the laser wavelength of 514 nm used in the laser light scattering experiments.

B. Light scattering setup

The experimental setup consisted of an Ar^+ laser, operating at a wavelength $\lambda=514$ nm, as light source, an ALV goniometer to adjust the scattering angle, and a fiber optic detector to measure the scattered intensity as a function of time. A commercial two lens setup (ALV) was used to reduce the natural width of the laser beam to a diameter of about 1 mm, the beam shining parallel on the sample. Intensity time correlation functions have been obtained from the homodyne detected scattered intensity using an ALV 5000 hardware correlator. The static small angle scattering pattern was viewed on a white screen in 200 cm distance from the sample, where a photograph could be taken (see below). All samples have been purified from dust by filtration with Millipore filters, pore-size 5.0 μm, and put into cylindrical Suprasil light scattering cuvettes of diameter 10 mm. During the measurement, the samples have been placed in a toluene bath of constant temperature 20 °C to avoid diffraction from the glass walls of the cuvettes, and to keep the sample temperature constant.

C. Unusual experimental phenomena

In light scattering experiments on these light absorbing colloidal dispersions several unusual phenomena, sketched in Fig. 3, have been encountered.

(1) Well-defined oscillations are found in the square root of the intensity autocorrelation function, $|F(q,\tau)|$, given by Eq. (1):

$$|F(q,\tau)|=G_2(q,\tau)^{0.5}=\left\{\int I(q,t)I(q,t+\tau)dt\right\}^{0.5}. \quad (1)$$

$G_2(q,t)$ is the intensity autocorrelation function; $I(q,t)$ corresponds to the scattered light intensity measured at time *t*. Those oscillations have been ascribed previously to convective motion of the tracers [10]. For a detailed study, our new tracer system *B* (see above) has been used, which shows more pronounced oscillations and also higher oscillation frequencies at identical experimental conditions (Fig. 4). The increase of the oscillation frequency in the intensity correla-

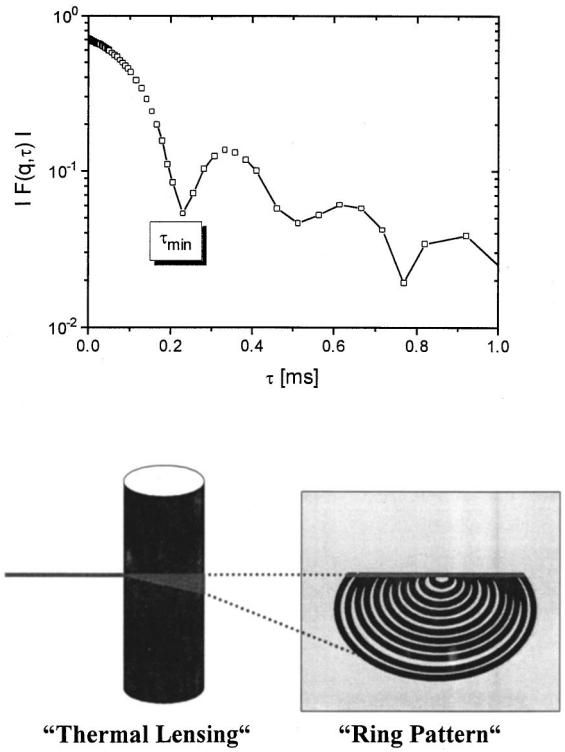

FIG. 3. Unusual phenomena encountered upon light scattering of light absorbing tracer particles, i.e., oscillations in the time intensity correlation functions (top), expansion of the incident laser beam and self-phase modulation (concentric rings) of the transmitted beam (bottom).

tion function for sample *B* corresponds to an increase of the convective flux velocity, which is a consequence of a larger amount of absorbed energy at a given laser power.

In the following sections, a detailed quantitative analysis will be provided, showing how the geometry of the convective flux can be deduced accurately from the dependence of the oscillations on the scattering angle. Also, the flux velocity itself will be determined.

(2) As shown in Fig. 3, the laser beam is expanded when entering the light absorbing dispersion. This effect, which is

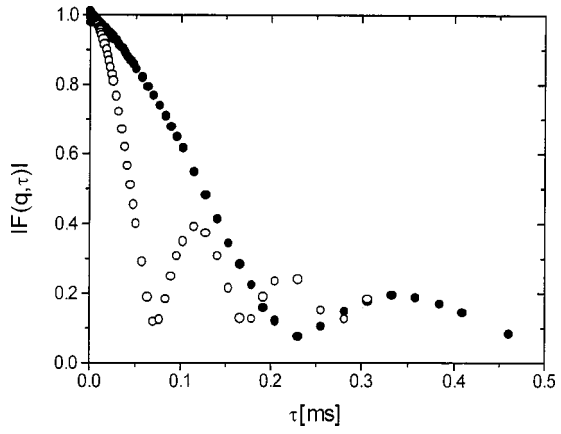

FIG. 4. Experimental time intensity correlation functions for tracer systems *A* (filled circles) and *B* (open circles), obtained at identical experimental conditions, i.e., laser power 500 mW and scattering angle 70°.

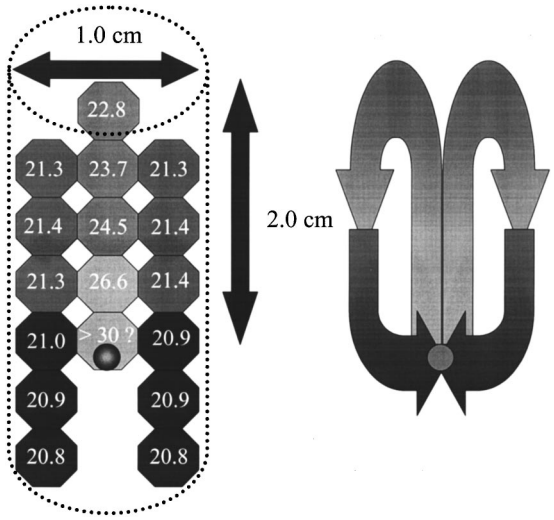

FIG. 5. Temperature profile within the sample cell (placed in a toluene bath at $T=20\,°C$, laser power 250 mW), measured with a Pt thermoelement, and resulting convection roll. The small circle corresponds to the cross section of the laser beam.

known as thermal lensing, corresponds to diffraction of light at a boundary separating regimes of different scattering power. As will be shown, these regimes are corresponding to warm and cold regions, containing different concentrations of tracer particles, respectively. The asymmetric distribution of particles in solution within a temperature gradient is known as Soret effect [14–16]. The variation in optical density with temperature causes a phase shift of the incident laser light, leading to a number of concentric rings in the profile of the transmitted beam. This pattern provides a direct measure for the spatial concentration distribution of the tracer particles, thereby allowing a quantitative determination of the Soret coefficient S_T [17]. Finally, it should be noted that the profile of the transmitted beam is not circular but asymmetric, which may be caused by gravitation, as will be explained later.

III. DYNAMIC LIGHT SCATTERING AND CONVECTION

A. Thermal profile and idealized scattering geometry

In Fig. 5, the local temperature profile within the sample, measured with a tiny cubic Pt thermoelement 1 mm in size, has been sketched. It should be noted that the temperature directly within the center of the laser beam cannot be measured because of light absorption of the Pt-element itself. Whereas the sample temperature beyond and alongside the incident laser beam remains nearly unchanged, there is a distinct temperature increase found perpendicular above the beam. The heating of the sample becomes less pronounced with increasing distance from the laser beam, until, at about 2.5 cm above the beam, the mean sample temperature of about 21 °C is reached. In the case shown in Fig. 5 (laser-power 250 mW), the temperature within the center of the beam obtained by interpolation should be higher than 30 °C. Therefore, the local maximum increase in temperature, ΔT, is about 10 °C at $P=250$ mW. The temperature profile as described corresponds to the convection pattern also sketched in Fig. 5: the sample is heated by the laser beam,

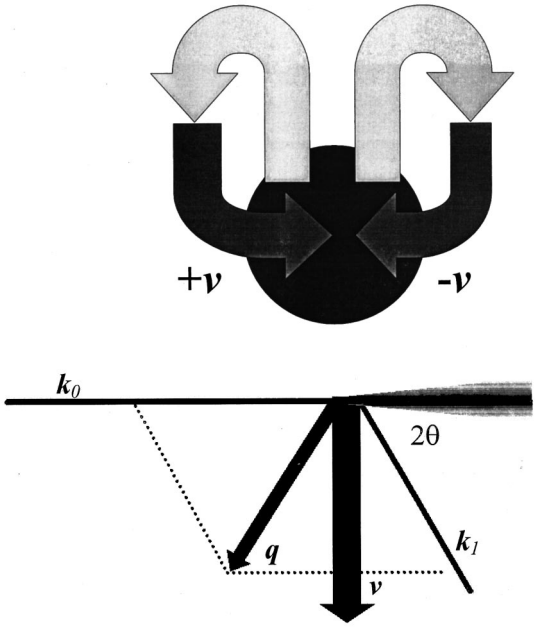

FIG. 6. Enlarged view of the convection roll already shown in Fig. 5, and a simplified sketch of the scattering geometry. See text for details.

leading to a decrease of the local density. As a consequence, the heated material is rising upwards, gradually cooling down after it has left the region of the laser beam, and flowing back at the edges of the sample cuvette. This convection roll, assuming a regular flux of scattering particles from the sample edges into the scattering volume, has direct consequences on the measured time intensity correlation function, $G_2(q,\tau)$.

Figure 6 shows an enlarged view of the convection roll, indicating the flux components visible in the light scattering plane with $+\mathbf{v}$ and $-\mathbf{v}$, and a simplified sketch of the actual scattering geometry. Only those components of the velocity vector $\mathbf{v}$ which lie within the scattering plane, which is defined by the incident laser beam $\mathbf{k}_0$ and the scattered beam $\mathbf{k}_1$, contribute to the measured signal.

B. Quantitative analysis of convection

In dynamic light scattering, regular motion of scattering particles with a given velocity vector $\mathbf{v}$ leads to a complex time amplitude correlation function [1]:

$$F(\mathbf{q},\tau)=\exp(i\mathbf{q}\cdot\mathbf{v}\tau). \tag{2}$$

$\mathbf{q}$ is the scattering vector shown in Fig. 6. In our case, scattering particles detected in the illuminated region are moving, in respect to the scattering plane, with velocities ranging from $-\mathbf{v}$ to $+\mathbf{v}$. Therefore, to solve the problem exactly, we have to calculate the integrate of Eq. (2) in the interval $-\mathbf{v}$ to $\mathbf{v}$. Here, we should mention that we make the plausible assumption that the convection roll is symmetric in respect to the incident laser beam, i.e., $|\mathbf{v}|=|-\mathbf{v}|$ (Fig. 6). The problem gets much more complicated if we also consider the diffusional or Brownian motion of the scattering particles; therefore [1]

$$F(\mathbf{q},\tau)=\exp(i\mathbf{q}\cdot\mathbf{v}\tau)\exp(-Dq^2\tau), \tag{3}$$

with D the self-diffusion coefficient of the particles. Importantly, D depends on the temperature of the dispersion according to the Stokes-Einstein relation:

$$D=\frac{kT}{6\pi\eta(T)R}. \tag{4}$$

kT is the thermal energy, $\eta(T)$ the temperature-dependent viscosity of the solvent, and R the hydrodynamic radius of the diffusing particles. Therefore, not only the flux velocity $\mathbf{v}$ of the scattering particles varies with position within the scattering volume, but also the diffusional relaxation time. For these reasons, an exact description of the oscillating correlation functions only is possible by integrating Eq. (3), considering as variables both temperature T and velocity $\mathbf{v}$. Since this integration is not practicable, we will concentrate mainly on the convection, which is responsible for the oscillations, and neglect the temperature (and position) dependence of the diffusion in the following. Considering the diffusional term to be independent of sample position, two different approaches for the oscillation correlations have been made.

(i) The velocity profile within the scattering volume should resemble a similar profile as the steady laminar flow field found in simple shear experiments. The main difference is that, in a shear experiment, the velocity ranges from 0 to v, whereas, in our experiment, it ranges from $-v$ to v. Also, in our case the velocity gradient is parallel to the flow itself, whereas it is perpendicular to the flow in a shear experiment. According to [18], in case of a simple shear experiment the homodyne correlation function measured by dynamic light scattering is given by

$$G_2(q,\tau)=\left[\frac{2J_1(\mathbf{q}\gamma L\tau)}{\mathbf{q}\gamma L\tau}\right]^2. \tag{5}$$

J_1 is the Bessel function of the first kind, L the cross-section dimension of the scattering volume ($L=1$ mm), and γ the velocity gradient vector within this cross section. It should be possible to describe the oscillating part of our experimental correlation functions using Eq. (5). Before we sketch an alternative more simplified approach, it should be noted that, as described by Eq. (5), the ''frequency'' of the oscillations scales with $\mathbf{q}\gamma$:

$$\mathbf{q}\gamma=\frac{4\pi n_D\sin(\theta)}{\lambda}\cos(\vartheta)\gamma=\frac{2\pi n_D}{\lambda}\sin(2\vartheta)\gamma. \tag{6}$$

n_D is the refractive index of the solvent, γ the absolute value of the velocity gradient. If Eq. (6) and the scattering geometry sketched in Fig. 6 are correct, the inverse of the first minimum in the correlation function should scale with $\sin(2\theta)$, 2θ being the total scattering angle.

(ii) Alternatively to the approach sketched in (i), we can restrict ourselves to the boundary conditions, i.e., consider scattering particles of flux velocity $+v$ and $-v$ only. In this case, the correlation function $F(q,\tau)$ is given by

$$\begin{aligned}F(q,\tau)&=[\exp(i\mathbf{q}\cdot\mathbf{v}\tau)+\exp(i\mathbf{q}\cdot-\mathbf{v}\tau)]\exp(-Dq^2\tau)\\&=2\cos(\mathbf{q}\cdot\mathbf{v}\tau)\exp(-Dq^2\tau).\end{aligned} \tag{7}$$

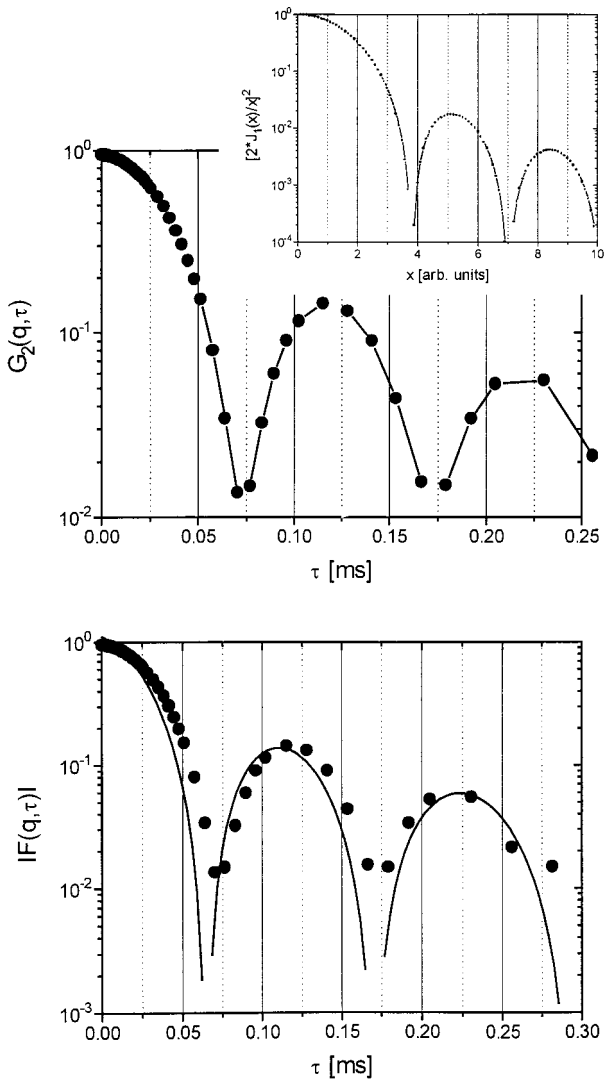

FIG. 7. Experimental data and fitting models for the oscillations caused by convection. (i) Fitting model based on the analogy of the convection velocity gradient to a simple shear experiment (top). (ii) Fitting model considering only the maximum convection velocities v and $-v$.

Similar to case (i), the oscillation frequency should scale with $\sin(2\theta)$ according to

$$\mathbf{q}\cdot\mathbf{v}=\frac{4\pi n_D \sin(\theta)}{\lambda}\cos(\vartheta)v=\frac{2\pi n_D}{\lambda}\sin(2\vartheta)v. \qquad (8)$$

Comparison of fitting models (i) and (ii). The best fits of the oscillations, obtained from sample *B* at laser power 500 mW and scattering angle $2\theta=70°$ (Fig. 4), are shown in Fig. 7. First, the reader should note that neither of the fitting functions describes the data accurately. However, the oscillation frequency itself is well fitted by both models. The fit according to model (i) [Fig. 7(a)] corresponds to a velocity gradient $\gamma=3.1\ \mathrm{s}^{-1}$. The cosine fit [Eq. (7) and Fig. 7(b)] yields a velocity $v=1.6\ \mathrm{mm\,s}^{-1}$. Taking into account the cross section of the scattering volume, i.e., $L=1$ mm, an average velocity gradient γ' can be calculated from the velocity v obtained by fitting model (ii), i.e., $\gamma'=2v/L=3.2\ \mathrm{s}^{-1}$. This value agrees remarkably well with the gradient $\gamma=3.1\ \mathrm{s}^{-1}$ [model (i)]. Therefore, it may be concluded that both models allow a quantitative estimate of the maximum flux velocity, which should be about $1.6\ \mathrm{mm\,s}^{-1}$ for the example shown in Fig. 7.

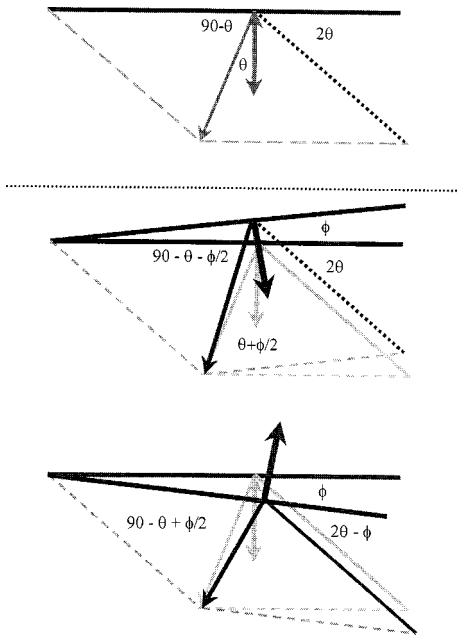

FIG. 8. Sketch of the changes in scattering geometry, which become necessary if the beam expansion is taken into account. The figure on top corresponds to the sketch shown in Fig. 6; the other drawings show the changes for velocity components $\mathbf{v}$ and $-\mathbf{v}$, respectively.

C. Effect of beam expansion on the scattering geometry

Both models discussed in the last section indicate that the oscillation frequency should scale with $\sin(2\theta)$. So far, the effect of beam expansion on the scattering geometry has been neglected (see Fig. 6). If we assume a beam expansion by an angle ϕ, the scattering geometry for particles flowing back into the scattering volume will change as sketched in Fig. 8. Here, it is assumed that the flow directions $\mathbf{v}$ and $-\mathbf{v}$ of the particles are always perpendicular to the incident laser beam.

According to Fig. 8, the angle between flow velocity $\mathbf{v}$ and scattering vector $\mathbf{q}$ changes from θ to $\theta+\phi/2$, the angle between $-\mathbf{v}$ and $\mathbf{q}$ from $180°-\theta$ to $180°-\theta+\phi/2$. Also, the scattering vector $\mathbf{q}$ itself has changed. This leads to

$$\mathbf{q}\cdot\mathbf{v}_1=\frac{4\pi n_D}{\lambda}\sin(\vartheta+\varphi/2)\cos(\theta+\varphi/2),$$

$$\mathbf{q}\cdot\mathbf{v}_2=\frac{4\pi n_D}{\lambda}\sin(\vartheta-\varphi/2)\cos(180-\theta+\varphi/2). \qquad (9)$$

Replacing the new scalar products [Eqs. (9)] into Eq. (7), it can be shown in a simple but lengthy calculation that the oscillation frequency should not scale with $\sin(2\theta)$, as in the idealized case neglecting beam expansion, but rather with $\sin(2\theta)+\sin(\phi)[1-2\sin^2(\theta)]$.

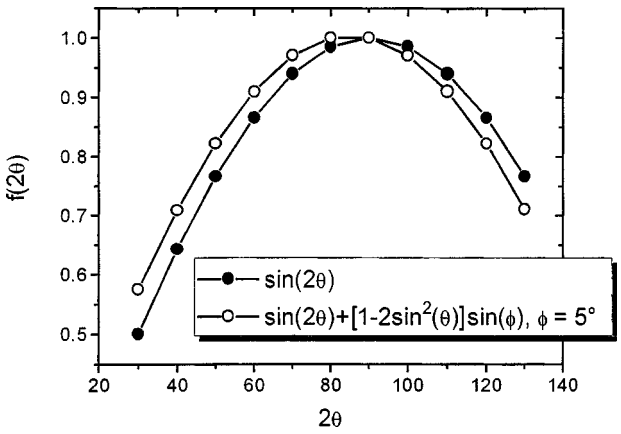

FIG. 9. Plot of the changed scaling function, which describes the dependence of the oscillation frequency of the correlation function on the scattering angle 2θ and the beam expansion angle ϕ.

Figure 9 shows that, for small ϕ, this change in q-scaling corresponds to a phase shift, in respect to 2θ, by the order of ϕ. We have checked these assumptions by determining the oscillation frequency for two different laser powers, i.e., two different beam expansions. Figure 10(a) shows the inverse first minimum, $\tau_{\min}$, plotted versus $\sin(2\theta)$, for a scattering angle ranging from 30° to 120°, laser power 500 mW. In this case, the maximum beam expansion $2\phi_0$ was 12.0°, corresponding to $\phi_0 = 6.0°$. Obviously, the data points do not scale with $\sin(2\theta)$, as assumed in the simple model neglecting the effect of beam expansion. In Fig. 10(b), the same data points are plotted versus $\sin(2\theta+5°)$. In this case, all data points fall nicely on a single line. Therefore, the oscillation frequency scaling indeed is shifted in phase, in respect to 2θ, by an angle the order of ϕ_0.

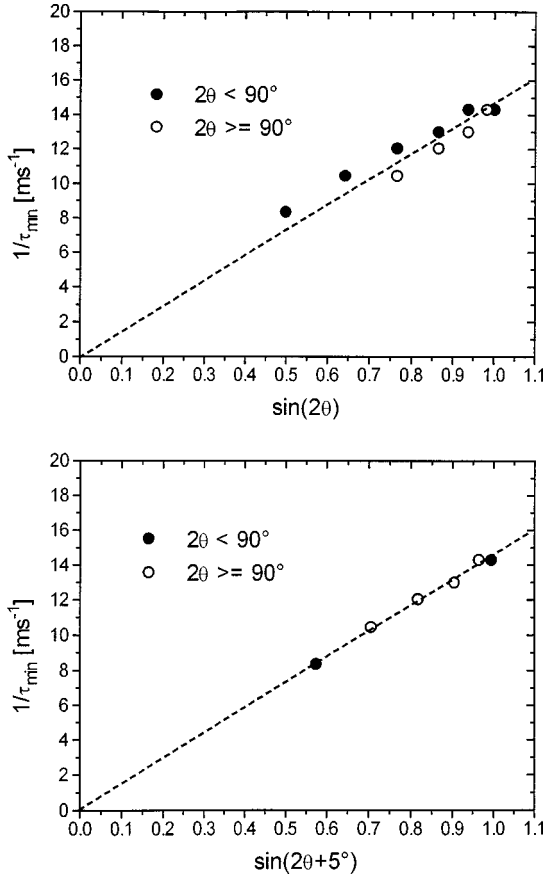

FIG. 10. Dependence of the inverse of the first minimum of the oscillations on scattering angle, neglecting beam expansion (top) and assuming a beam expansion $\phi = 5°$ (bottom). Experimental data obtained at $P = 500$ mW, maximum beam expansion $2\phi_0 = 12°$.

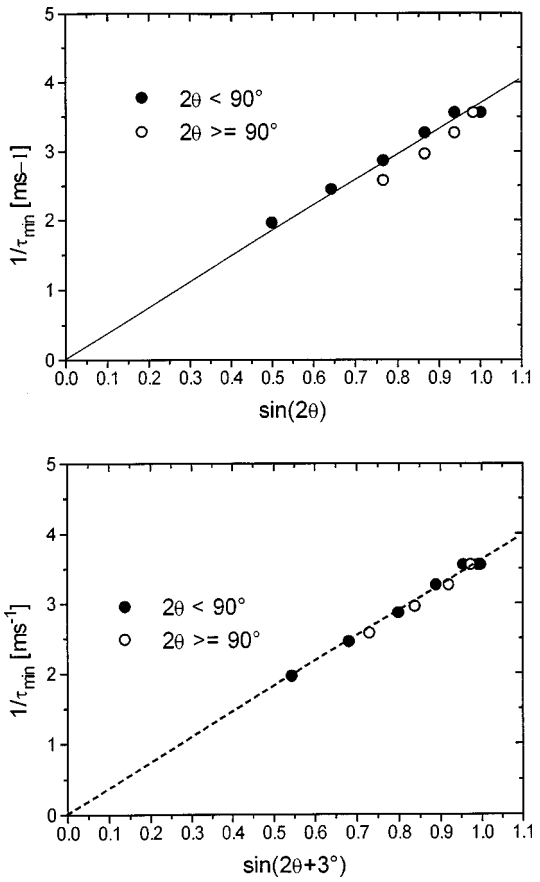

FIG. 11. Same as Fig. 10, with $P = 100$ mW and maximum beam expansion $2\phi_0 = 6°$. Here, the data could be fitted with $\phi = 3°$ (bottom).

At a smaller laser power of 100 mW and, consequently, smaller energy input and local heating of the sample, the total beam expansion $2\phi_0$ was 6.0°. In this case, the phase shift necessary to allow a linear fit of the data points was $3° = \phi_0/2$, as shown in Fig. 11.

Those results prove the assumptions made in Fig. 8, concerning the necessary changes in scattering geometry due to expansion of the incident laser beam. Finally, it should be noted that we have assumed a continuous linear expansion by a constant angle ϕ. In practice, the expansion angle is continuously increasing within the light absorbing sample. However, since the sample dimension and the maximum expansion angle are rather small, the actual beam expansion ϕ at the location of the scattering volume should be comparable to or only slightly smaller than the maximum beam expansion ϕ_0. This corresponds nicely to the results shown in Fig. 10, where the phase shift was 5° compared to a maximum beam expansion $2\phi_0 = 12°$.

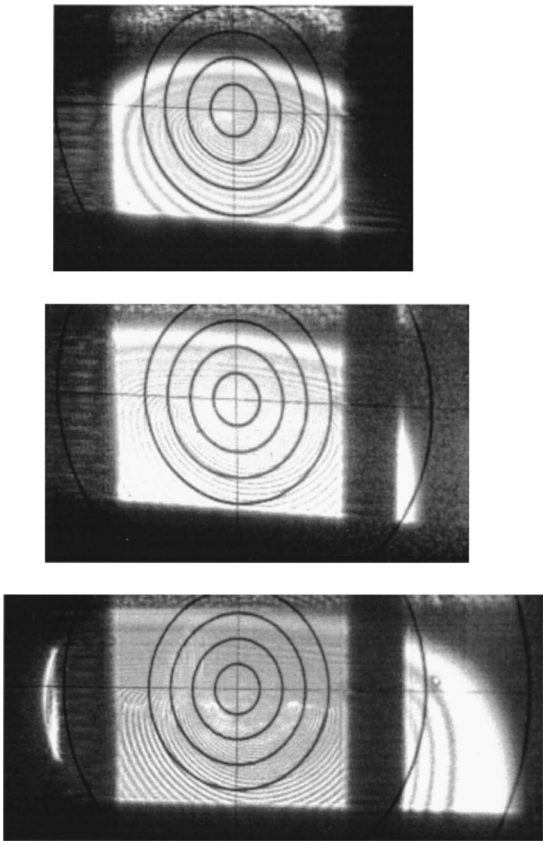

FIG. 12. Photographs of the concentric ring profile of the transmitted beam, obtained for $P=100$, 200, and 300 mW (from above).

IV. TRANSMITTED BEAM PROFILE—SORET EFFECT AND GRAVITY

A. Soret coefficient from the maximum phase of the transmitted beam profile

Figure 12 shows the profile of the transmitted laser beam, photographed from a scattering screen in 200 cm distance from the sample, obtained for three different laser powers. With increasing laser power not only the beam expansion but also the number of concentric rings, i.e., the maximum phase shift Φ_0 in the transient laser light, increases. According to [17] [Eq. (48)], the dependence of the maximum phase shift Φ_0 on laser power P should provide a direct measure for the Soret coefficient S_T:

$$\Phi_0=-\frac{2\pi L}{\lambda}\frac{x}{1+x}[(dn/dc)_T-1/S_T(dn/dT)_c], \quad (10)$$

with the factor x given by

$$x=\frac{\sigma_0 S_T P}{\pi \lambda_T}. \quad (11)$$

L is the dimension of the scattering volume, λ the wavelength of the incident light, dn/dc and dn/dT the variation of the refractive index of the dispersion with solute concentration and temperature, respectively. All these quantities should be independent of laser power P. The factor x, however, depends on laser power, Soret coefficient, absorption constant σ_0 and the product of specific heat capacity and temperature conductivity of the solvent, λ_T [$=0.123$ W/(m K) for cyclohexane]. For a 0.2 wt. % solution of tracer B in cyclohexane, $\sigma_0=1.1\ \mathrm{cm}^{-1}$. The number of concentric rings, which is proportional to the maximum phase shift Φ_0, was 18, 28, 33, and 36 at $P=25$, 50, 75, and 100 mW, respectively. According to Eqs. (10) and (11), S_T can be calculated from the dependence of the number of diffraction rings on laser power P. The increase in number of concentric rings N_{CR} with laser power P is given by

$$N_{\mathrm{CR}}=K\frac{x}{1+x}. \quad (12)$$

Here, the factor K summarizes all factors given in Eq. (10) which should be independent of laser power. Therefore, K itself also should be independent of P. The only quantity varying with P is our new variable x given in Eq. (11). To obtain the Soret coefficient, we have to know the number of concentric rings for different laser powers, and in addition the absorption coefficient of our tracers σ_0 and the product of specific heat capacity and temperature conductivity of our solvent λ_T. In this case, each laser power—concentric ring number relation corresponds to an equation with the unknown quantities K and S_T. Having determined at least two of those equations, both these quantities can be calculated. As an important consequence, it seems not to be necessary to know the refractive index increments dn/dc and dn/dT to get the Soret coefficient.

For tracer B, we obtained a Soret coefficient $S_T(B)=0.06\ \mathrm{K}^{-1}$. Analogous, we determined the Soret coefficient for tracer A from the dependence of the number of diffraction rings on laser power, i.e., $S_T(A)=0.07\ \mathrm{K}^{-1}$. These values correspond quite well to S_T of colloidal particles of about 100 nm in size in aqueous dispersion [19], i.e., $S_T=0.05$–$0.1\ \mathrm{K}^{-1}$. For polymer particles in organic solution, which are, oppositely to our tracers, swollen by the organic solvent, the Soret coefficient found in literature is about one order of magnitude larger, i.e., $S_T=0.3\ \mathrm{K}^{-1}$ [20]–$1\ \mathrm{K}^{-1}$ [21]. At present, our tracer systems are investigated by thermo forced Rayleigh scattering [20] to check the Soret coefficients obtained by our simple method. Note, however, that for this technique the refractive index increments have to be determined separately.

B. Influence of gravity on the diffraction pattern

If we compare our experimental Soret pattern, shown in Fig. 12, with the pattern suggested in [17], there is an obvious difference: whereas the theoretical pattern should be strictly spherical, the experimental pattern is asymmetric. As already mentioned above, this deviation could be caused by the effect of gravity. Like shown in Fig. 13, immediately after shining the laser beam on the absorbing sample a spherical symmetric pattern, corresponding to a symmetric temperature profile, was observed (b). Within 1–2 seconds, this pattern deforms to become asymmetric (c). The deformation corresponds to an analogous deformation of the temperature profile within the sample, caused by a decrease of solvent density with increasing temperature. In a gravity

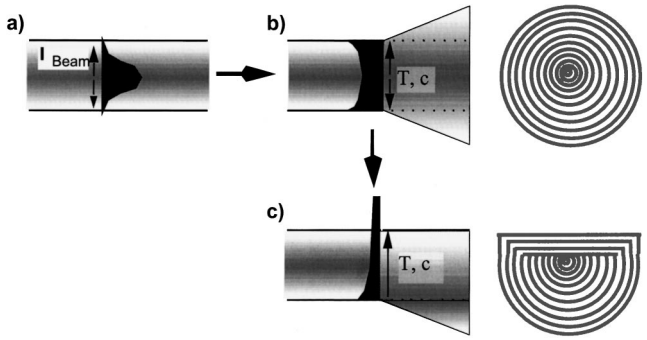

FIG. 13. Intensity profile of the laser beam (a) and resulting density profiles of the sample immediately after illumination (b) and a few seconds later, when the symmetric profile has deformed probably due to the effect of gravity (c).

field, heated regions of the sample are rising towards the sample surface, thereby cooling down and flowing downward again along the sample edges, and a convective roll pattern is established. Since it takes some time for the material to cool down, the sample temperature is distinctly increased even a few centimeters above the laser beam (Fig. 5). Consequently, the temperature gradient responsible for the beam expansion (thermal lensing) is much less steep in upward direction compared to sideways or downward, leading to an asymmetric beam expansion (c). Under microgravity conditions, one would expect the circular pattern shown in Fig. 13(b) and theoretically described [17] to remain stable, and no convection roll should develop.

Finally, it should be noted that deformed concentric ring patterns of the transmitted laser beam recently have been found also for liquid crystals (LC) undergoing transverse motion [22,23]. Although the reason for the concentric pattern in this case was not the Soret effect as assumed for our isotropic system, but the large optical anisotropy of the LC, the deformation might have similar reasons, i.e., the influence of uniform motion on the isotropic self-phase modulation. According to Fig. 3 shown in [23], the deformation of the ring pattern is largest in the direction opposite to the motion direction. Therefore, in our case the deformations shown in Fig. 12 would indicate a motion direction from top to the bottom of the sample. This is in contrast to the convection roll model (Figs. 5 and 6), where the main flux direction is from the scattering volume to the top of the sample as also emphasized by the experimental temperature profile. Therefore, here we assume that motion of the sample has much less influence on the deformation of the concentric ring pattern than a Soret effect within an asymmetric temperature profile caused by gravity effects.

V. CONCLUSIONS

In this paper, we have presented a detailed analysis of oscillations found in time intensity correlation functions of dynamic light scattering experiments on light absorbing colloidal particles. The oscillations correspond to convection flux of the scattering spheres, created by light absorption and local heating of the sample, as has been confirmed independently by measurements of the local temperature within the sample. Remarkably, the increase in temperature in the scattering volume, i.e., the center of the laser beam, is 10 °C (250 mW) or even larger, depending on laser power. From the dependence of the oscillation period on the scattering angle, the convection flux direction within the scattering plane could be deduced: the scattering particles are flowing perpendicular upward from the heated region, flowing back alongside the sample edges after cooling down, and reentering the scattering volume from aside. It is these components of backflow from aside, i.e., within the scattering plane defined by the propagation vectors of the incident and the scattered laser beams, which are detected in the dynamic light scattering experiment. Importantly, the expansion of the laser beam has to be taken into account to describe the dependence of the oscillations on the scattering angle accurately. On the other hand, the angular dependence of the oscillations provides an independent measure of the beam expansion angle at position of the scattering volume. It should be noted that it has not yet been possible to develop a mathematical fitting function to describe the experimental data accurately. This is due to the fact that the problem is extremely complicated, i.e., the signal contains two modes of particle motion, thermal convection and Brownian motion, both of which should depend on position within the scattering volume. Nevertheless, neglecting the position dependence of the Brownian motion by assuming a constant diffusion coefficient D, fitting functions to describe the oscillating part of the correlation function satisfactory have been obtained. This semiquantitative analysis of the correlation functions yielded a maximum velocity of about 1.6 mm/s at laser power 500 mW.

In addition, the transmitted beam showed a typical concentric ring pattern predicted in literature [17], which has been used to determine the Soret coefficient for our tracer particles. Importantly, this self-phase modulation is deformed asymmetrically in contrast to the sketch shown in [17]. This deformation may be caused by gravity, which deforms the thermal profile within the sample via formation of a convection roll. The effect of convection on the concentric ring pattern so far had been neglected.

In summary, we have shown how laser light scattering can be used to study simultaneously various quantities as particle diffusion, thermal diffusion (Soret effect) or flux velocity in convection rolls. As a future work, it would be interesting to carry out a dynamic light scattering experiment on light absorbing particles under microgravity conditions, where no or a totally different convection pattern should be found. Also, the study of microscopic (length scale about 1 μm) and macroscopic (length scale about 1 mm) viscosity, given by diffusion coefficient and flux velocity, respectively, in complex fluid systems is possible with our new tracer system. Using laser light of a different wavelength at low intensity, the convection oscillations may be suppressed, and the diffusion coefficient is readily determined from a simply exponential correlation function.

ACKNOWLEDGMENT

Financial support from the Materials Science Center of the University Mainz is gratefully acknowledged.

[1] R. Pecora, *Dynamic Light Scattering* (Plenum Press, New York, 1985).
[2] B. Chu, *Laser Light Scattering* (Academic Press, New York, 1992).
[3] P. N. Pusey, in *Liquids, Freezing and the Glass Transition*, Les Houches Sessions LI, edited by D. Levesque, J. P. Hansen, and J. Zinn-Justin (Elsevier, Amsterdam, 1990).
[4] S. G. Stanton, R. Pecora, and B. S. Hudson, J. Chem. Phys. **75**, 5615 (1981).
[5] W. Schaertl, C. Graf, and M. Schmidt, Prog. Colloid Polym. Sci. **104**, 129 (1997).
[6] L. M. Liz-Marzan and A. P. Phillipse, J. Colloid Interface Sci. **176**, 459 (1995).
[7] F. Baumann, M. Schmidt, B. Deubzer, M. Geck, and J. Dauth, Macromolecules **27**, 6102 (1994).
[8] F. Baumann, B. Deubzer, M. Geck, J. Dauth, S. Sheiko, and M. Schmidt, J. Adv. Mat. **9**, 955 (1997).
[9] F. Baumann, B. Deubzer, M. Geck, J. Dauth, and M. Schmidt, Macromolecules **30**, 7568 (1997).
[10] W. Schaertl, C. Roos, and K. Gohr, J. Chem. Phys. **108**, 9594 (1998).
[11] H. Benard, Ann. Chim. Phys. **23**, 62 (1901).
[12] S. H. Davis, J. Fluid Mech. **30**, 465 (1967).
[13] H. J. Palmer and J. C. Berg, J. Fluid Mech. **47**, 779 (1971).
[14] H. J. Eichler, P. Guenther, and D. W. Pohl, *Laser-Induced Dynamic Gratings* (Springer-Verlag, Berlin, 1986).
[15] D. W. Pohl, Phys. Lett. **77A**, 53 (1980).
[16] W. Koehler, J. Chem. Phys. **98**, 660 (1993).
[17] N. V. Tabiryan and W. Luo, Phys. Rev. E **57**, 4431 (1998).
[18] G. G. Fuller, J. M. Rallison, R. L. Schmidt, and L. G. Leal, J. Fluid Mech. **100**, 555 (1980).
[19] P. M. Shiundu, G. Liu, and J. C. Giddings, Anal. Chem. **67**, 2705 (1995).
[20] W. Koehler and P. Rossmanith, J. Phys. Chem. **99**, 5838 (1995).
[21] M. E. Schimpf and J. C. Giddings, Macromolecules **20**, 1561 (1987).
[22] N. V. Tabiryan, S. R. Nersisyan, and M. Warenghem, Phys. Rev. Lett. **77**, 3355 (1998).
[23] N. V. Tabiryan, S. R. Nersisyan, and M. Warenghem, J. Appl. Phys. **83**, 1 (1998).